Static friction and adhesion in polymer–polymer microbearings

Z. Rymuza [a,*], Z. Kusznierewicz [a], T. Solarski [a], M. Kwacz [a], S.A. Chizhik [b,1], A.V. Goldade [b,2]

[a] *Faculty of Mechatronics, Institute of Micromechanics and Photonics, Warsaw University of Technology, ul. Chodkiewicza 8, 02-525 Warsaw, Poland*
[b] *Metal–Polymer Research Institute of Belarussian Academy of Sciences, Kirov Street 32a, 246652 Gomel, Belarus*

Abstract

The starting process, i.e., transition from static to kinetic friction in polymer–polymer microbearings, was studied. Load, sliding speed and time of contact before starting were varied during the experiments. AFM studies of rubbing surfaces were performed and the real surfaces were brought into contact in computer simulations to evaluate the adhesive and frictional interactions. Correlation between observed static friction force, adhesive force and calculated friction force characteristics vs. time was found. © 2000 Elsevier Science S.A. All rights reserved.

Keywords: Static friction; Adhesion; Polymer–polymer microbearings

1. Introduction

Polymer–polymer microbearings are often embodied in modern miniature devices. Polymer components are very cheap and their manufacture by moulding in the production process is very effective. Application of many, mostly thermoplastic polymers, is not often optimised. Tribological behaviour of polymer–polymer journal microbearings is not well known [1–3]. It pertains to, in particular, very important starting process of the bearing when the transition from static to kinetic friction occurs. This process is extremely important in Micro Electro Mechanical System (MEMS) bearings [4–6].

The process of transition from static to kinetic friction is rarely studied [7]. The period of the preliminary displacement in a tribosystem when the static friction force increases can lead to the critical situations when drive system in a device can not move the driven element because of too high friction resistance. Such problem is very important in polymeric bearings, particularly in MEMS bearings, where surface forces and rheological properties of materials of rubbing elements play important role. The time of static contact of rubbing elements before sliding effects significantly on the static friction force during the transition to sliding.

To understand the role of various operational conditions and the design of the bearing on the characteristic curve friction force (or coefficient) — time of sliding during the start of a polymer–polymer microbearing — a series of frictional measurements was carried out.

2. Experimental

The journal microbearing shown in Fig. 1 was investigated. Several material combinations were studied. The materials used for moulding of the bearing bush are listed in Table 1. The shaft was manufactured from polyamide (PA) 6 with 25% glass fibre (GF) (see no. 8 in Table 1).

Tests of the transition from static to kinetic friction were performed in laboratory conditions using the test rig described in detail elsewhere [3]. Three parameters were varied during the experiments: load, sliding speed and time of previous contact before rotation of the shaft. The load

---
* Corresponding author. Tel.: +48-22-660-8540; fax: +48-22-660-8601; e-mail: kup_ryz@mp.pw.edu.pl
[1] E-mail: spm@spm.polymer.gomel.by.
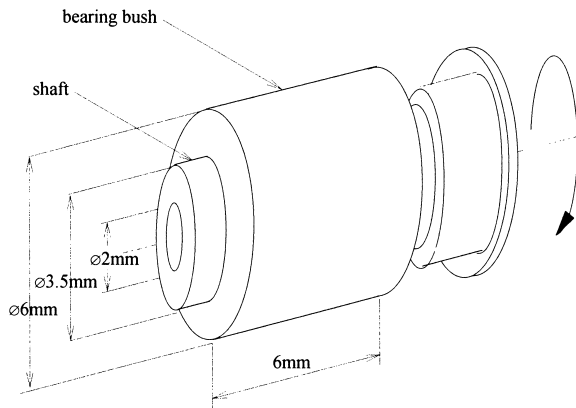[2] E-mail: spm@spm.polymer.gomel.by.

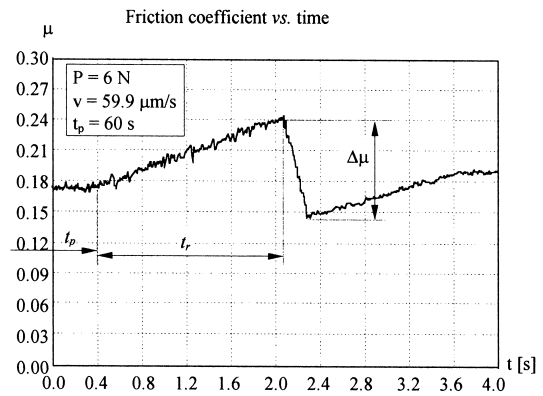Fig. 1. The polymer–polymer microbearing under study.

Fig. 2. Example of typical graph of friction coefficient vs. time during transition from stationary contact to sliding; shaft ϕ 3.474 mm, bearing bush ϕ 3.560 mm, materials 8 (PA6 + 25%GF)-shaft and 1 (PS)-bearing bush (Table 1), respectively.

was in the range of 6–30 N, sliding speed 1.2–101.6 μm/s and time of preliminary contact 1–900 s.

3. Results of experimental studies

The characteristic curves describing the period of transition from static to kinetic friction obtained from the experiments can be presented by typical one characteristic shown in Fig. 2. It can be observed that the process of preliminary displacement in the bearing is accompanied by the significant friction force/coefficient increase. The increase of the friction coefficient $\Delta\mu$ and time needed to sliding t_r can be treated as principal frictional characteristics of the starting process.

The analysis of experimental results shows that at variation of load P, sliding speed v and time t_p of static contact of the bearing bush and journal (shaft) before rotation of the shaft, the friction coefficient (Figs. 3–7) and the time needed for sliding (Figs. 8 and 9) increase significantly at the increase of time of previous static contact under load before the rotation of the shaft (before experiment). As the sliding speed increases, a decrease in

time t_r is observed but the friction coefficient does not change significantly. The effect of load both on the friction coefficient and the time needed for sliding is small.

The time t_r needed to slide the shaft on the bearing bush surface of the studied polymer–polymer microbearing can be estimated using the following analysis. It is known [10,11] that the complex adhesion parameter Δ_a can be used to estimate the adhesion ability of a rigid rough contact.

$$\Delta_a = \frac{3}{4} \frac{1}{\sigma R^{1/3}} \left(\frac{\pi R \Delta\gamma}{E'} \right)^{2/3} \tag{1}$$

when E' (see Eq. (6)), interfacial surface free energy $\Delta\gamma$, and average statistical value of roughness are known (σ is the root-mean-square deviation of height, R is the average radius of microasperities).

The complex adhesion parameter is the ratio of adhesive force acting on a single asperity as the effect of surface forces to the reactive force of rigid single asperity.

At the estimation of the preliminary displacement l in a microbearing until the start of sliding, it is reasonable to

Table 1
Materials used for the manufacture of bearing bushes (1–8) and shaft (8) of tested microbearings
GF: Glass fibre, h: homopolymer, c: copolymer.

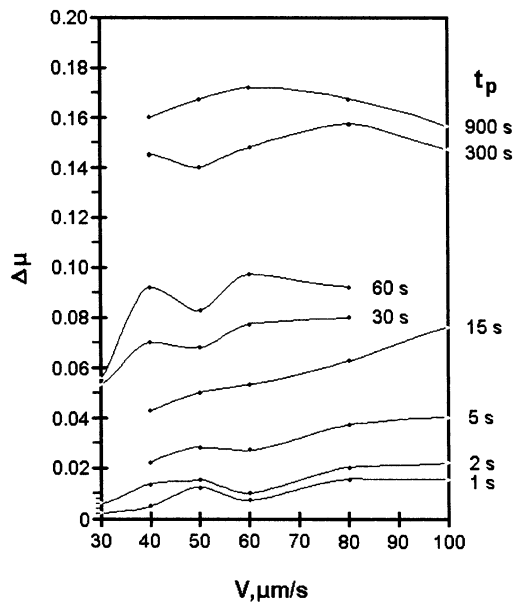|	ISO symbol of polymer	Material	Surface free energy, γ [mJ/m^2]	Momentary elasticity modulus, E_0 [MPa]	Poisson's ratio, ν	Micro-hardness, HB [MPa]	Shear strength, σ_s [MPa]
1	PS	Polistyren KM	44	2700	0.34	120	40
2	PA6	Tarnamid T-27	46	1600	0.35	75	40
3	PA11	Rilsan	35	1500	0.35	75	38
4	POM h	Delrin AF	35	1800	0.34	130	55
5	POM	Delrin 500	38	2300	0.34	160	65
6	PETP	Arnite 160	43	1800	0.34	100	45
7	POM c	Tarnoform 300	40	1800	0.34	130	50
8	PA6 + 25%GF	Itamid 253	112	3500	0.32	100	55
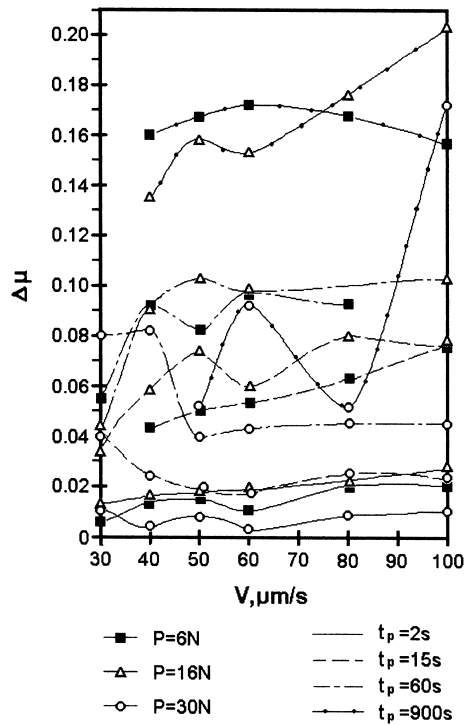
Fig. 3. Increase of friction coefficient at transition from stationary contact to sliding vs. sliding speed at various times of stationary contact before experiment under loads 6, 16 and 30 N; for microbearing, see Fig. 2.
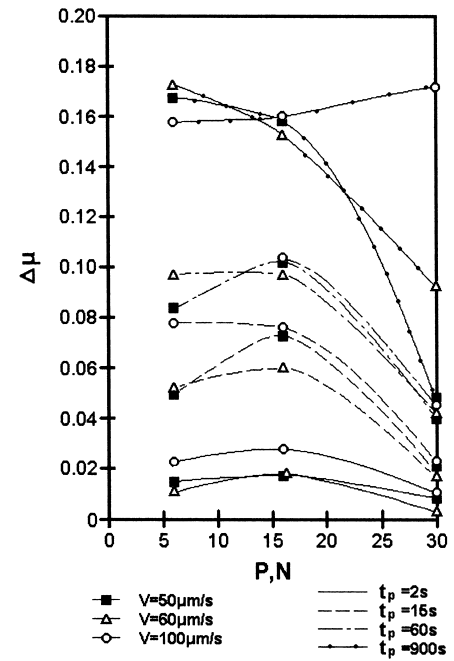

Fig. 5. Increase of friction coefficient at transition from stationary contact to sliding vs. load and times of stationary contact before experiment; for microbearing, see caption to Fig. 2.

use, instead of the roughness parameter σ, a characteristic length l_0 for the whole contact region. Then

$$l = l_0 \Delta_a \tag{2}$$

The time of the elongation of the material until the length l is reached depending on the velocity of deformation of the

material ν_d, which also depends on the sliding speed ν. The last relationship can be assumed to be linear, so

$$\nu_d = c\nu \tag{3}$$

where c represents the constant value.

Fig. 4. Increase of friction coefficient at transition from stationary contact to sliding vs. sliding speed at load $P = 6$ N at various times of stationary contact before experiment; see caption to Fig. 2.
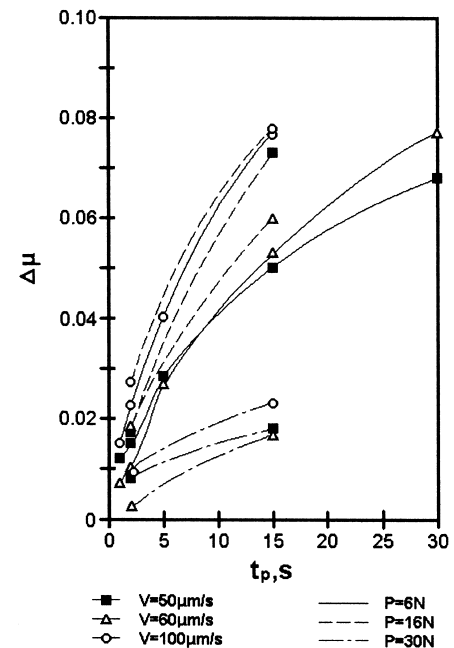

Fig. 6. Increase of friction coefficient at transition from stationary contact to sliding vs. time of stationary contact before experiment at various sliding speeds and applied loads; for microbearing, see caption to Fig. 2.
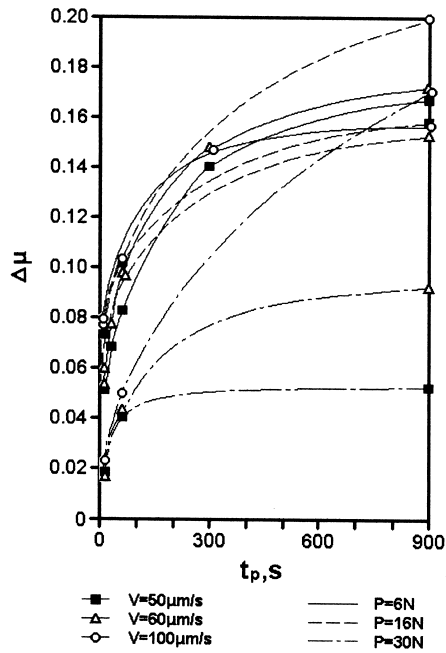
Fig. 7. Increase of friction coefficient at transition from stationary contact to sliding vs. time of stationary contact before experiment at various sliding speeds and applied loads; for microbearing, see caption to Fig. 2.

Fig. 9. Time needed for sliding vs. sliding speed at load $P = 6$ N and various times t_p of stationary contact before experiment; for microbearing, see caption to Fig. 2. Material PA11 (Rilsan). Theoretical equations are Eqs. (1)–(4). Assumed values of parameters are $E_0 = 1500$ MPa, $t_0 = 70$ s, $\delta = 0.7$, $P = 16$ N.
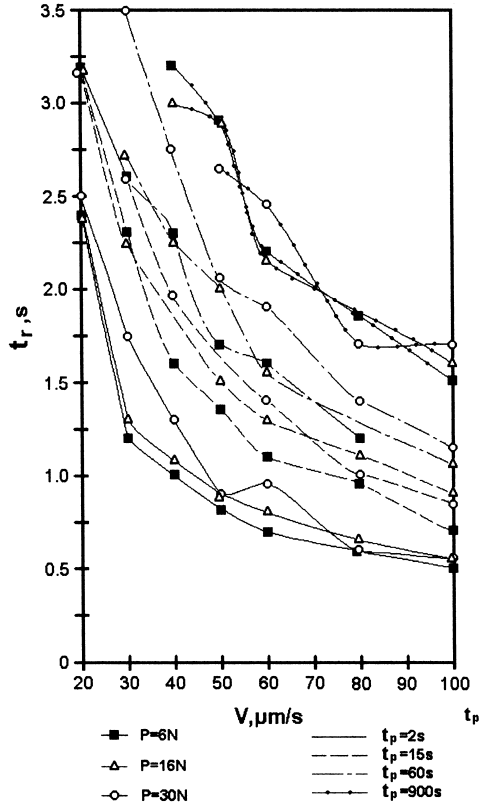

Fig. 8. Time needed for sliding vs. sliding speed at various loads and times of stationary contact before experiment; for microbearing, see caption to Fig. 2.
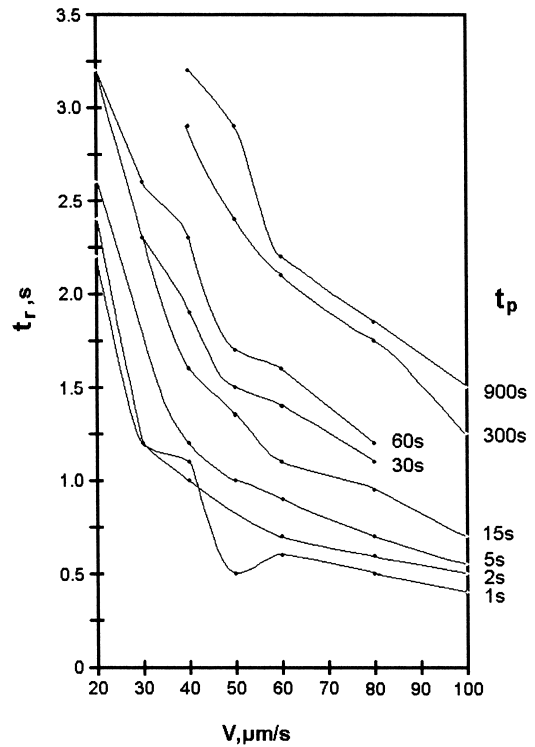
The time t_r for the preliminary displacement between the contacting surfaces in the bearing before sliding may be estimated as follows

$$t_r = l/\nu_d = \frac{l_0}{c}\frac{\Delta_a}{\nu} \tag{4}$$

The time t_p at calculations of t_r is considered by the elasticity modulus, which is in Δ_a (Eq. (1)), and is time-dependent according to Eq. (5).

Taking into consideration the variations of the elasticity modulus as a function of time t_p of the static contact at $l_0/c = 40$ μm, $E_0 = 1500$ MPa (most elastic material PA11 (Rilsan), $t_0 = 70$ s, small $\delta = 0.7$, load 16 N), we can find the graphs shown in Fig. 10. The calculated values of t_r correlate with the values found determined experimentally (Figs. 8 and 9).

The results of the experiments allow us to assume that the frictional behaviour of the bearing in transition from static contact to sliding of the rubbing elements depends on the rheological behaviour of polymeric materials during the process of formation and destruction of rubbing surfaces. Such assumption was a basis for the construction of a model of contact of rubbing surfaces for, as minimum,
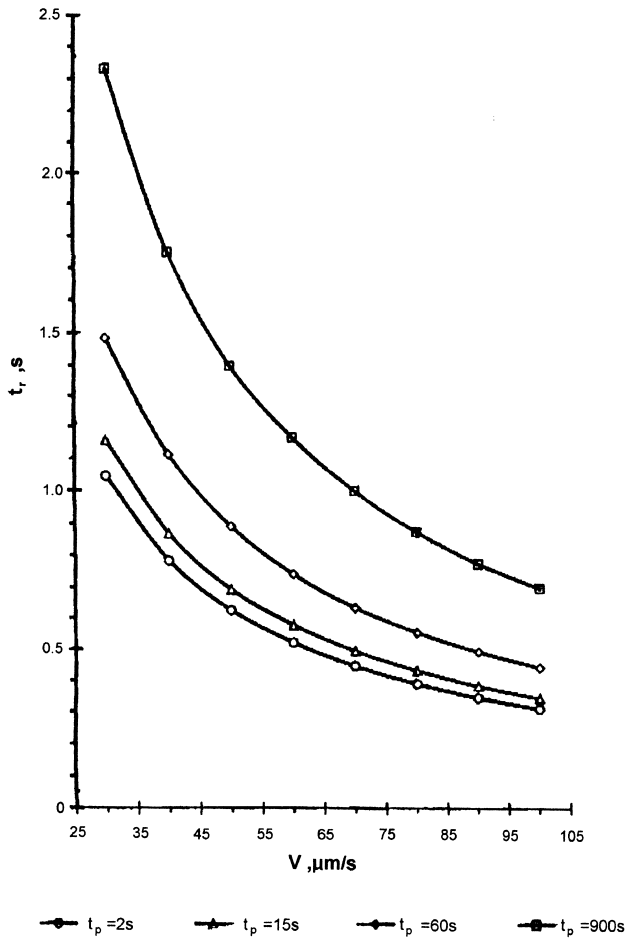
Fig. 10. Theoretically found time t_r needed for sliding vs. sliding speed at various times t_p of stationary contact before the experiment; for microbearing, see caption to Fig. 2. Material PA11 (Rilsan). Theoretical equations are Eqs. (1)–(4). Assumed values of parameters are $E_0 = 1500$ MPa, $t_0 = 70$ s, $\delta = 0.7$, $P = 16$ N.

qualitative description of the process of formation of real (actual) contact (RAC) of materials with strong effect of rheological behaviour as a function of time of previous contact before sliding and also to clear the change of RAC during the transition from static to kinetic friction.

4. Model of contact and discussion

The shape and size of the RCA depend on the topography (roughness) of the rubbing surfaces, mechanical properties of materials and the load characteristics (load and time). The construction of the model of contact is, likewise, not easy because of the need to consider simultaneous variation of elasticity of the material and the roughness of the surface during the formation of RCA (as a function of time of loading). This is why, for such a problem, it is difficult to use the statistical models of rough contact of Greenwood–Williamson type, where the approximation of the tips of microasperities using simple geometrical shapes

(spheres, ellipsoidal segments, conical shapes, etc.) is applied. In such situations, it is reasonable to apply a model of the rough contact [8], in which, without additional idealisation, we can consider the effect of micro- and nanoroughness of contacting surfaces, and it is also possible to obtain easy transition (''frozen'') state of topography for every discrete time interval when the modulus of elasticity of the material is well-defined during the process of RAC formation.

The rheological behaviour of polymeric materials in a microcontact is poorly investigated. At the selection of function of time dependence of elasticity modulus, it is necessary to use the formulae for macrovolumes of polymeric materials. At viscoelastic stress the following formula for elasticity modulus will be applied:

$$E = E_0 - \delta E_0 \left(1 - e^{t/t_0} \right) \tag{5}$$

where E_0 is the value of momentary elasticity modulus, t_0 is characteristic time of relaxation (retardant time), $\delta = (E_0 - E_\infty)/(E_0)$, E_∞ is relaxation elasticity modulus, and t is time.

The above formula was found taking into consideration the viscoelasticity functions equivalent to the viscoelastic Voight's element [9]. Here, also the Boltzmann's principle of superposition is taken into consideration. Fig. 11 shows the graphs, which give the influence of various parameters, used in Eq. (5) on the elastic modulus of the material. The momentary value of the elasticity modulus E_0 defines the base value of considered mechanical characteristics of the materials (t_0 indicates velocity and δ is the magnitude of its rheological changes).

Parameters δ and t_0, which describe the process of viscoelastic contact deformation of microasperities, are very difficult to measure without finding the original test procedures. It was the reason why in the carried-out calculations, only the approximate estimation of fundamental characteristics of the materials were used which, of course, does not change the qualitative description of the contact. For every type of polymeric material, the viscoelastic characteristics of the material can vary upon the well-known curves [9].

It may be assumed that the friction coefficient, as a function of time during the static contact before experiment and at the preliminary displacement (during experiment), is influenced by the rheological processes. Taking into consideration this assumption, the method of comparison of the results of the calculation of RAC with parameters of the friction characteristic curve given in Fig. 1 was used to find approximate values of δ and t_0.

The characteristic times of relaxation in static conditions can be significantly higher than at shear load. Taking into consideration the Boltzmann's superposition principal, we assume that at the transition to sliding the deformation effects of normal and tangential loads summarise.
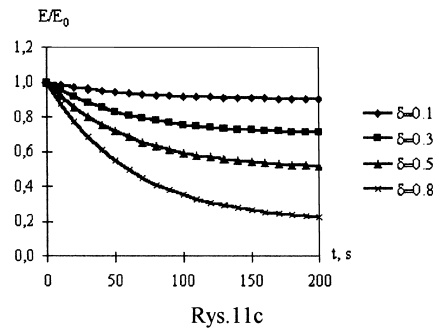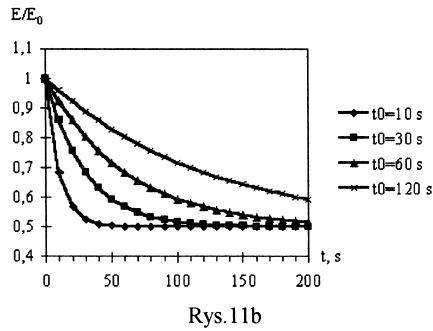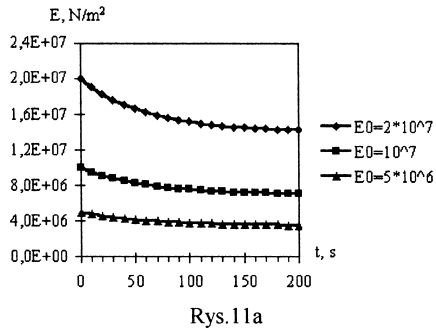
Rys.11a

Rys.11b

Rys.11c

Fig. 11. Rheological dependencies of elasticity modulus vs. time at various values of: momentary elasticity modulus E_0 — (a), relaxation time t_0 — (b) and parameter δ — (c). In (b) and (c), ratios of E/E_0 are given.

For the characterisation of the contact between the shaft and the bearing bush the equivalent elasticity modulus was used

$$E' = \left(\frac{1 - \nu_1^2}{E_1} + \frac{1 - \nu_2^2}{E_2} \right)^{-1} \qquad (6)$$

The energy of adhesion was calculated as follows:

$$\Delta\gamma = \gamma_1 + \gamma_2 - \gamma_{1,2} \qquad (7)$$

where the surface free energies with the numbers 1 and 2 relates to the shaft and bearing bush materials, respectively, and $\gamma_{1,2}$ is interfacial energy.

The values of E_0, ν, σ_s (see Table 1) relate to the macrovolume of material. The properties in a thin layer may be different, so at the solution of the problem of the formation of RAC the data given in Table 1 can be used for comparative, not absolute, estimation of the studied bearing characteristics.

For the applied model of contact of rough realistic surfaces it was necessary to obtain the 3D images of the topography of the contacting surfaces. The use of traditional contact profilometers for polymeric materials is not reasonable because of possible destruction of the surface by the tip of a profilometer. The application of Atomic Force Microscopy (AFM) at relatively large scanning area is more effective [12]. The AFM 10×10 μm scan images were used as the base topography data in computer calculations of RAC.

To study the polymeric materials using AFM, it is necessary to apply a special procedure [11]. To obtain 3D AFM images of topography of used polymeric elements, the AFM operating in dynamic non-contact mode was applied. It was possible, therefore, to find the topography images at relatively long distance of the tip from the investigated surface (to several tenths of nanometers). The resolution in such a method is not high (0.1–0.2 nm in normal directions and 2–5 nm in tangential directions, respectively) compared with the contact mode operation. However, at preliminary studies it was found that at the contact of microasperities with height below 1–2 nm, the continuum area of contact of the discrete polymeric surfaces occurs [8]. Therefore, for the description of the polymer–polymer contact the topography measurements with nanometric resolution of the height of the microasperities were applicable.

The AFM studies of the polymeric materials were performed for the samples listed in Table 1. When the characteristic relief for the tested material was found, therefore, the typical images for the investigated sample of bearing bush and shaft were used for computer simulations of contact.

The visualisation of the results of scanning was performed by 2D and 3D topography images. For every type of visualisation, the contrast grey imagining of the surface relief in peaks (white colour relates to the highest peaks, black to the deepest valleys) or in angles, when the effect of illumination is modelled (more light are the elementary elements of topography for which the angle of normal direction has lower differentiation with the angle of the light ''illumination''). Also, the statistical analysis of the peaks was performed and the local angle of inclinations of microasperities was found. The average values of the topography parameters can be used to compare the quality of the surfaces and in the statistical models of a rough contact (Table 2). The AFM images were made on the rubbing surfaces and the direction of friction force is along the y-axis shown on the images in Table 2.

The maximum height H on the scan size and root-mean-square deviation of height was selected as characteristic parameters (see Table 2). Local angles inclinations are averaged (α_m) for every elementary area of AFM images; they were also characterised by most frequently found angle α_v. The surface anisotropy coefficient k_a is 1 for strongly anisotropy surfaces and 0 for the surface with the

material elongated in one direction. These parameters are given for every image. The characteristic scan area was 10×10 μm; every image is described with the proper scan area used for the tested material.

The conclusion relating to the AFM images of the tested elements is such that the rubbing surfaces are characteristic with nanoroughness in the same range. The highest local angles of inclination of the microsperities of the surface relief correspond with the surfaces with most dispersed elements of the surface topography (samples 1 and 4). The surfaces of the samples 2 and 4 are most isotropic for which the form of topography elements are close to spherical. The more anisotropic are the surfaces of the samples 1, 3 and 6, for which the form of asperities is strongly elongated on nanoscale (sample 1) or on microscale (samples 3 and 6).

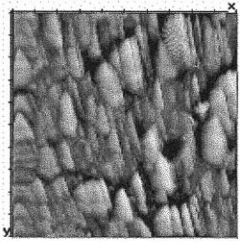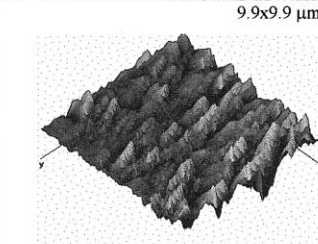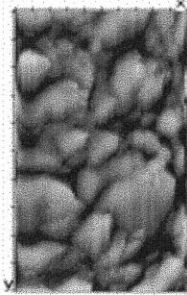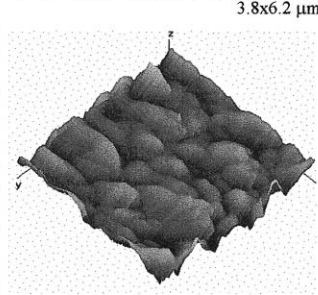Table 2

Characteristics of topography of rubbing surfaces

Material	AFM images		Heght parameters	Angle parameters	Anisotropy coefficient
	2-D	3-D			
1	2	3	4	5	6
1. Polistyren KM		9.9x9.9 μm	$H=355.6$ nm $\sigma=36.5$ nm	$\alpha_m=10.5°$ $\alpha_v=5.5°$	$k=0.17$
2. Tarnamid T-27		3.8x6.2 μm	$H=163.6$ nm $\sigma=18.7$ nm	$\alpha_m=7.7°$ $\alpha_v=3.8°$	$k=0.50$
3. Rilsan		7.3x7.3 μm	$H=184$ nm $\sigma=21.8$ nm	$\alpha_m=12.2°$ $\alpha_v=3.2°$	$k=0.18$
4. Delrin AF		9.1x9.9 μm	$H=352$ nm $\sigma=28.1$ nm	$\alpha_m=14.2°$ $\alpha_v=5.1°$	$k=0.42$
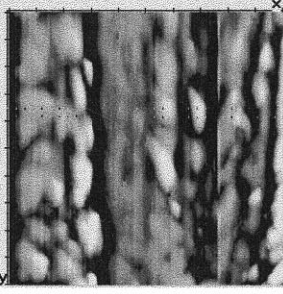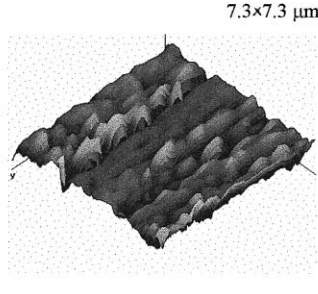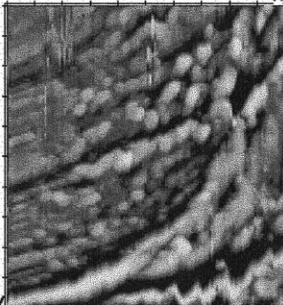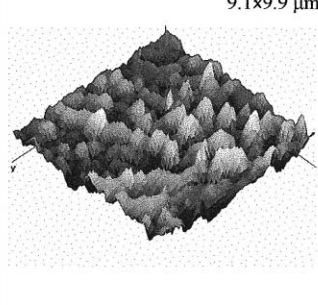
Table 2 (continued)
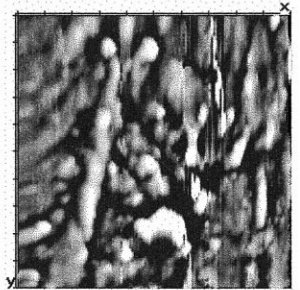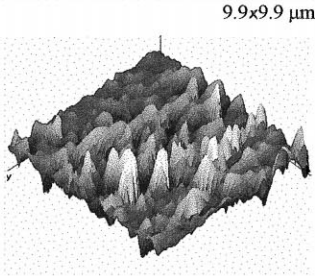
1	2	3	4	5	6
5. Delrin 500		9.9×9.9 μm	$H=317.4$ nm $\sigma=35$ nm	$\alpha_m=9.2°$ $\alpha_v=3.1°$	$k=0.38$
6. Arnite A160		8.6×7.3 μm	$H=228$ nm $\sigma=32.7$ nm	$\alpha_m=8.9°$ $\alpha_v=2.0°$	$k=0.20$
7. Tarnoform 300		6.7×7.3 μm	$H=286.8$ nm $\sigma=26.6$ nm	$\alpha_m=8.4°$ $\alpha_v=2.8°$	$k=0.23$
8. Itamid 253		6.9×9.9 μm	$H=403.3$ nm $\sigma=44.1$ nm	$\alpha_m=8.3°$ $\alpha_v=2.2°$	$k=0.29$
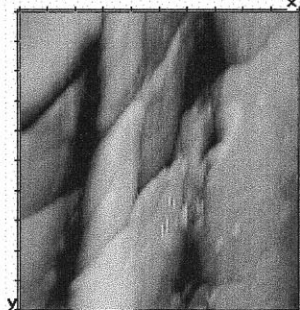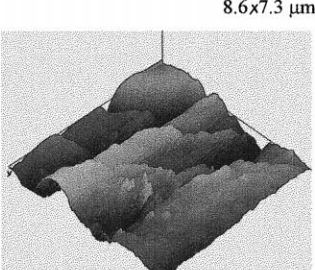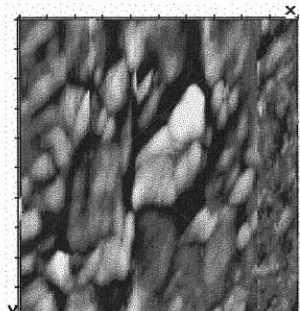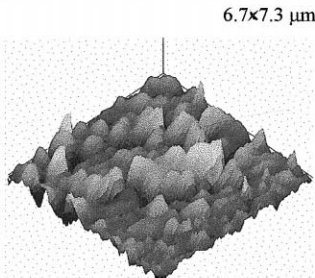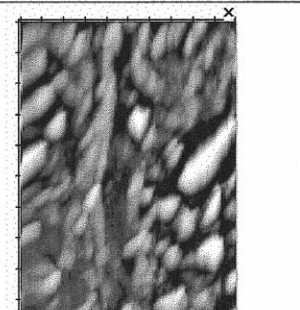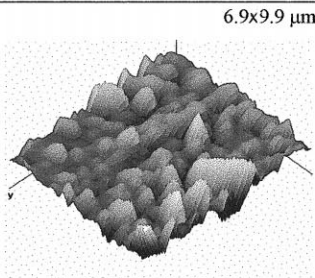
The obtained 3D AFM images were used in computer modelling of the contacting surfaces of the tested microbearing. The use of stochastic models for the description of a rough surface leads to a significant idealisation of the surface and, in particular, does not include the structure of the relief on the direction of the valleys. The full spatial representation of the topography of the surface is possible using the peaks function $Z(x, y)$, which in numerical form is spatial presentation of Scanning Tunnelling Microscopes (STM)/AFM image of the surface on the investigated area.

On the first stage of the construction of the model, a force interaction of the fragment of the solid surface having the height of the relief $z_i = Z(x_i, y_i)$ measured in the characteristic points of the net of scanning and idealised, flat solid surface is considered. For the pin (asper-

ity) having the height dependent on z_i in the point (x_i, y_i), the force resistant to deformation is a function of the magnitude of approaching

$$P_i(\delta_i) = \frac{E'}{kh_{\max}}\delta_i \qquad (8)$$

where $k = (1 + \nu)(1 - 2\nu)/(1 - \nu)$; $h_{\max}$ is normalised length parameter, which may have the physical sense as the thickness of the deforming layer.

The adequate description of the contact behaviour of the surfaces separated with the gap of nanometer size is not possible without considering the interface interactions, which particularly for ''soft'' materials (e.g., polymers), are large enough. The molecular interactions of surfaces we will characterise through the potential of Lennard–Jones $F_i = f(l_i)$, where l_i is the gap size.

The shape of deforming surface is described by press in the contact points and elongation dz_i outside the area of contact, which can be find from the force balance on the elementary area of the surface

$$dz_i = \frac{8}{3}\Delta\gamma kh\varepsilon^2 E'^{-1}l^{-3} \qquad (9)$$

For the new surface, $z_i' = z_i + dz_i$ is possible to calculate compressive and tensile stresses in every contact point. After summarising the stresses, we can obtain nominal contact stress P_d and specific adhesion force F_s:

$$P_d(h) = \frac{4}{3}E'\Delta x\Delta y\Sigma(h - z_i) \qquad (10)$$

$$F_s(h) = \frac{8}{3}\Delta\gamma\varepsilon^2\Delta x\Delta y\Sigma(h - z_i)^{-3} \qquad (11)$$

Because the assumed deformation h usually is not that of equilibrium location of the surfaces, the force equivalent to the stress and elongation forces

$$P = F_s(h) + P_d(h) \qquad (12)$$

is not zero and, depending on the direction (plus or minus), relates to external stress force or the force acting for separation of the surfaces, which is needed for equilibrium of the surfaces in the state adequate to the approach h of the surfaces. For the solution of the inverse problem by selecting h adequate to the external load P, it is possible to define the location of the surfaces in realistic contact under load and RAC for the defined deformation h. The RAC in such situation can be described as

$$A_r = nd x d y \qquad (13)$$

where n is the number of points in contact where

$$z_i > h$$

On the second stage of the construction of the mode,l there is considered a contact of two rough surfaces. The calculation of a discrete contact of two rough surfaces is a relatively complex problem of statistic modelling. Its solution reduces to the definition of the parameters of an equivalent surface, or to the definition probability function of the contact of surfaces.

The problem may be simplified significantly if we have numerical functions of the microasperities of the surfaces $Z_1(x, y)$ and $Z_2(x, y)$ entering into contact. In our case, such functions are the files of 3D AFM images of the surfaces of the bearing bush and shaft. For the computer analysis of contact of two rough surfaces, we selected fragments with rubbing surfaces bearing the same physical dimensions and the dimensions of the matrix of images according to the scans along axes x and y. The mutual covering of the surfaces defines the contact at normal approach of the surfaces set of pairs of points being in indirect contact. The contact occurs only for the points (i, j) for which the following condition is fulfilled

$$Z_1(i,j) + dZ_1(i,j) + Z_2(i,j) + dZ_2(i,j) < h \qquad (14)$$

where $dZ_1(i,j)$, $dZ_2(i,j)$ represents the increase in number of microasperities caused by adhesive interactions, h is the distance between the levels for calculation of the height of points in the used AFM images and the adequate level of approach of the discussed surfaces. The picture of the contact points of the surfaces Z_1 and Z_2 on the plane XY can be treated as RAC of an equivalent surface

$$Z'(i,j) = Z_1(i,j) + Z_2(i,j) \qquad (15)$$

with an absolutely flat surface when the deformation is h.

Because the average local inclination angles of microasperities on the nanometer scale are very small (not greater than several degrees), the sum of the contact areas (RAC) $S + nd x d y$ is adequate to the area of contact of two rough surfaces. Here, n is the number of contacting pairs of points of AFM images for which condition (14) is fulfilled.

The problem of modelling of contact of two rough surfaces reduces to the model of contact of equivalent rough surface, to which refers the sum (Eq. (15)) of AFM images, with an absolutely flat surface. The result of application of such a model the is visualisation of RAC, forces of molecular interactions and stresses of deformation of the materials during contact (Fig. 12) and also the quantitative description of their characteristic parameters.

On the third stage of the construction of the computer model of polymer–polymer contact, it is possible to take consider the peculiarities of the viscoelastic deformation of materials. The contact formation process in such a case occurs as follows. Under the external load P of two rough surfaces the viscous flow of material, which according to the rules of relaxation processes is possible to treat as a decrease of elasticity modulus of the material ($E_i < E_{i-1}$). To obtain equilibrium with the external load N the additional deformation of material, leading to a new deformation of microasperities h_i. The result of the additional deformation of the rough layer is calculated and visualised using the computer model.
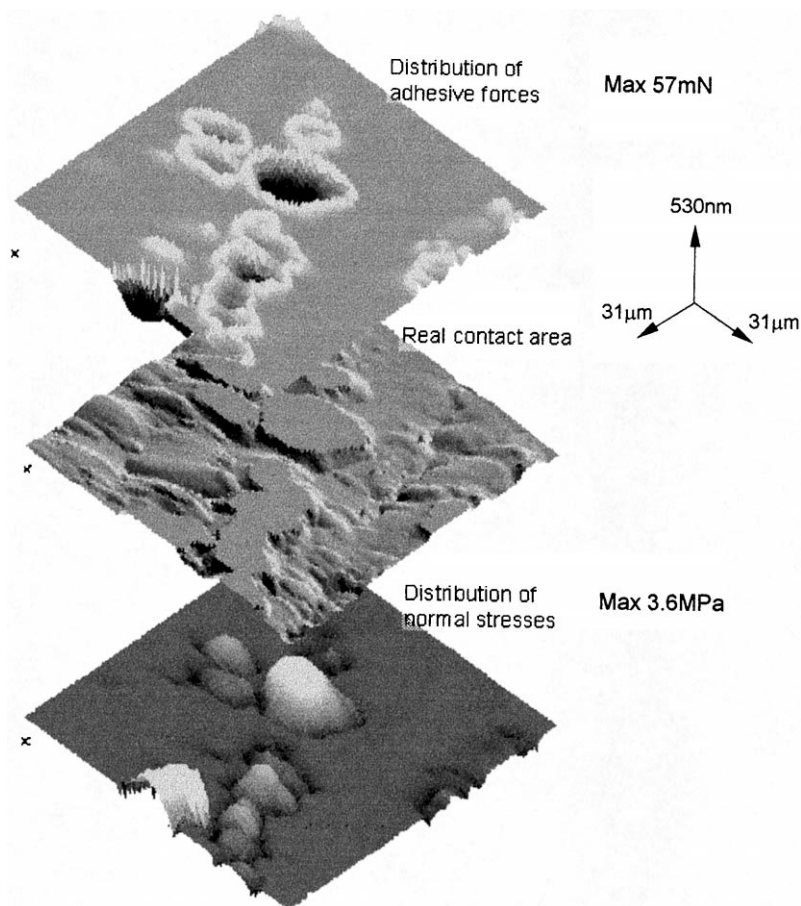
Fig. 12. Results of visualisation of modelling of adhesive contact.

As the result of decrease of elasticity modulus, i.e., decrease of rigidity of material, the contact zone, which on the step $i-1$ was equilibrated, is now no longer in the equilibrium state. An additional deformation of the material leads to the increase of the bearing contact area, which is formed as the effect of the deformation of microasperities. The process of the formation of contact as a function of time can be characterised by the time-dependent set of the relative locations of contacting surfaces, which can be described by the following parameters: deformation h_i for every moment time, RAC A_i and the image Z_i for the relief after its deformation in the defined period of time.

The numerical realisation of the presented picture of the formation of the viscoelastic rough contact is possible to perform with the following algorithm.

1. At elasticity modulus E_0 and initial topography of an equivalent surface, Z' using the computer model is possible to calculate the deformation of the rough layer h_0 and real area of contact A_0, adequate to the external load P, and the image Z'_0 can be found which characterises deforming relief in the initial stage $t = 0$.

2. The time period for the next i-th interval $t_i = t_{i-1} + t$ is selected. The magnitude of elementary time interval Δt

can be selected on every step, i.e., the time interval may vary.

3. The momentary elasticity modulus E_i is calculated using the formula

$$E_i = E_0 - \delta E_0 (1 - e^{-t_i/t_0}) \tag{16}$$

4. The deformation h_i and RAC A_i are calculated for the roughness given by the image Z'_{i-1} taking into consideration the new value of elasticity modulus E_i and the external load P. The image Z'_i characterising the relief for every i-th period of its deformation.

5. When it becomes a necessity to analyse a contact during a very long period of time, a return to item (2) of this algorithm is needed. In every succeeding step of calculations, the initial image of deformed relief obtained in the previous step is used. For every i-th calculation step the elasticity modulus E_i, which fulfils the laws of relaxation processes, i.e., $E_i < E_{i-1}$. As the result of decrease in the elasticity modulus, i.e., decrease of rigidity of the material, the contact zone, which on $i-1$ step was equilibrated, will be unstable. The external load P equilibrated by the additional deformation of the material leads to the new deformation level of the microasperities h_i.

The effect of additional deformation of the rough layer is calculated and visualised using a program realisation of the computer model.

As an example of the use of the computer model, the contact of the materials 1 (PS) and 3 (PA11) used for the bearing bushes and material 8 (PA6 + 25%GF) for the shaft (see Table 1) was considered. The selected materials are the ''hardest'' (1 — $E_0 = 2700$ MPa) and the ''softest'' ones (3 — $E_0 = 1500$ MPa). The results of modelling for these materials can characterise the behaviour of the contacts in a wide range of viscoelastic properties. We can consider, as the example of parameters characterising viscoelastic behaviour of materials, the following quantities: for material 1 — $\delta = 0.3$, $t_0 = 100$ s; for material 3 — $\delta = 0.7$, $t_0 = 70$ s. For material 3, the viscoelastic properties are more distinctly expressed than in material 1.

Because for the polymer–polymer contacts the most reliable mechanism of friction is adhesive, the friction force is proportional to actual area of contact A

$$F_{ad} = \sigma_s A \qquad (17)$$

Because it is reasonable to assume that the shear strength σ_s is constant during the low-speed process of transition from static friction to sliding, the time-dependent characteristics of RAC can be studied. The calculation was carried out for the adequate AFM images $Z(i, j)$, which characterise equivalent surface of contact of two rough surfaces. An example of construction of the image for the equivalent surface of the contacting surfaces $3 + 8$ is shown in Fig. 13. The calculation of images in every step of deformation in the contact was then realised using the computer model. The visualisation of the process of increase of relative area of contact is shown in Fig. 14. For every interval of time, there corresponds a relative value of RAC, i.e., A/A_a, where A_a is nominal area equal to the area of the scan fragment.

The results of the calculations are shown in Fig. 15, where the dependence of the relative RAC as a function of time as the surfaces enter into contact under various external loads P, can be observed. The rapid increase of RAC in initial stage of loading at the increase of load occurs and the scale of the rheological changes in the contact increases. At very high loads, the RAC will be close to its maximum value so the rheological increase of RAC will be small. The comparison of the results of
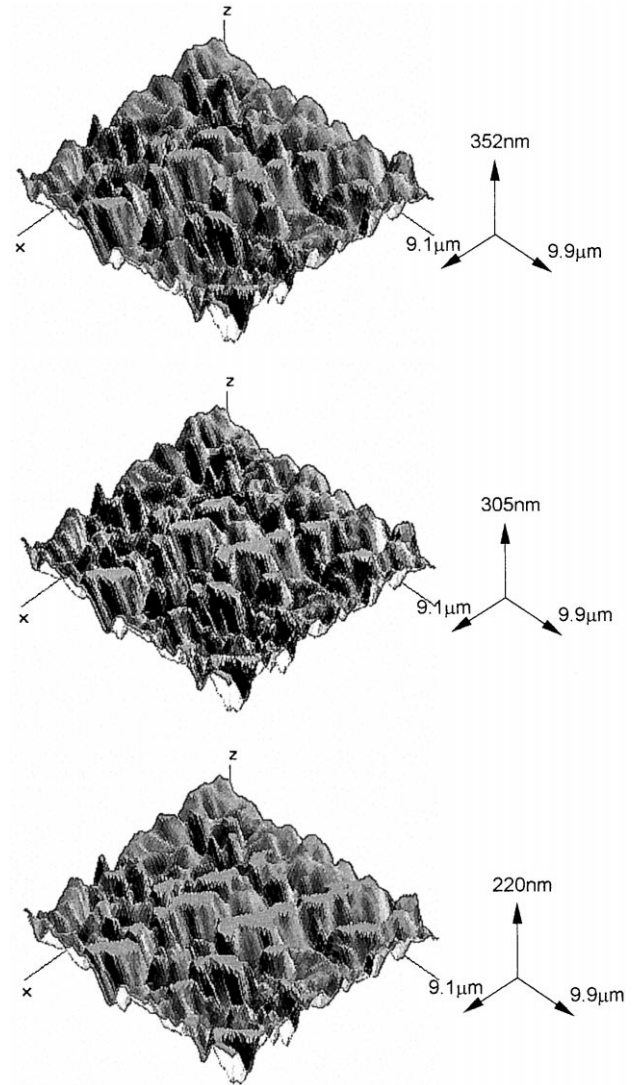

Fig. 14. Visualisation of the process of increase of relative real area of contact of viscoelastic contact for various times of stationary contact: 15 s (a), 60 s (b), 900 s (c).

calculations for various fragments of the surface of the tested element (Fig. 15) demonstrates their similarity and shows the possibility of the description of the contact using characteristic AFM images. The results for the materials 1 (PS) and 3 (PA11) are shown in Fig. 15. The
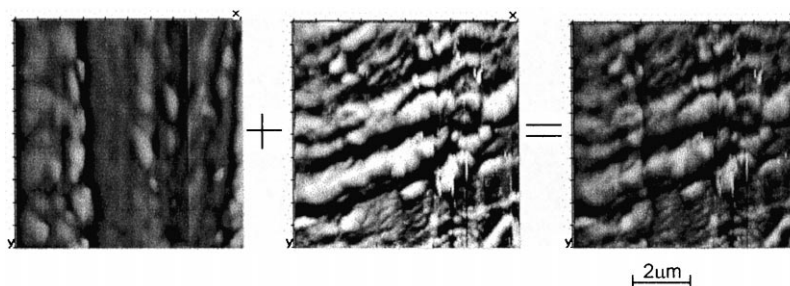

Fig. 13. Summarising of images of fragments of bearing bush and shaft surfaces for the construction of equivalent surface.
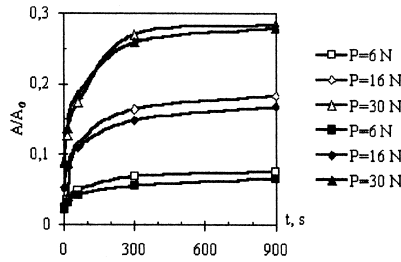
Fig. 15. Dependence of calculated relative real area of contact on time of stationary contact before sliding at various external loads; comparison for surfaces of materials 1 and 3 (see Table 1). A_a: Nominal area of contact.

difference is caused not only by various reliefs in the surface topography but mainly because of the elastic properties of the materials and the parameters of their viscoelastic behaviour. In the initial stage of contact at small external loads, and/or for the materials with high rigidity the contact occurs only as a result of the deformation of the heights microasperities. In that case, even at viscous flow of the materials the rapid increase of RAC is not observed (Fig. 15, curves for $P = 6$ N). For more rigid material 1 at low load the RAC is almost constant.

The increase of the friction coefficient as a function of the previous contact time based on the experimental data as compared with the calculation results is shown in Fig. 16. The experimental and calculation curves are very close. A decrease in parameter $\Delta\mu$ is observed as the load is increased. The function is, however, non-monotonous.

For more quantitative comparison of the calculation and experimental results, a correction of the calculation results was carried out. The analysed quantity was the following parameter

$$\Delta\mu_c = k' \frac{A - A_0}{P} \qquad (18)$$

where A_0 is RAC observed at $t = 0$, k' is coefficient relating the shear stress of the weaker material — the value of k can be found by the comparison of the calculation and experimental results at $P = 30$ N. The comparison of the calculation and experimental results of the increase of friction coefficient at various loads and at the influence of the rheological phenomena is presented in Fig. 16. The presented model describes not only the time characteristics
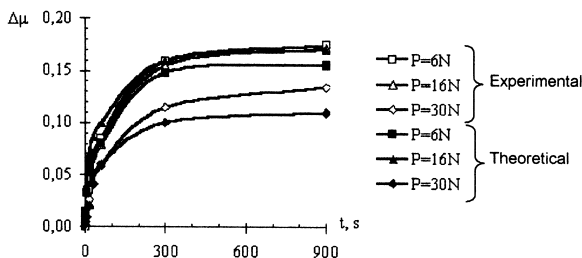

Fig. 16. Comparison of experimental and theoretical data of increase of friction coefficient on time of stationary contact before sliding at various loads. Material PA11 (Rilsan).
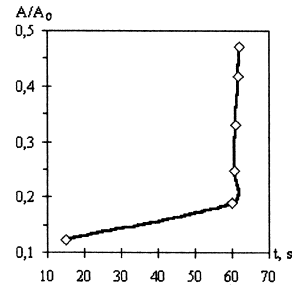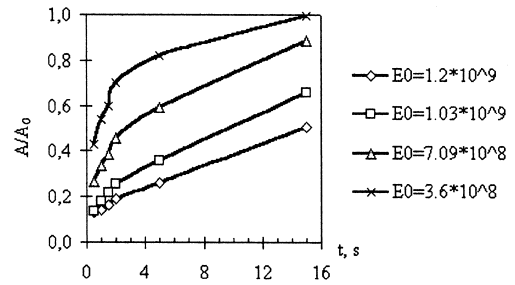

Fig. 17. Time dependence of relative area of contact at various parameters: elasticity module (a), at change of rheological parameters during transition to sliding (b).

of the friction coefficient but also the tendency of decrease of friction coefficient at the increase of load.

The process of the transition from the stationary state to sliding is very complex. The influence of the shear stresses on the rheological behaviour of the materials is very distinct [10]. When the frictional load is applied, the rheological process is activated and for its description, quite new values of δ and t_0 should be used. In Fig. 17a, the relationships for a new phase of the rheological increase of RAC at application of the shear stresses during the various moments of the static contact, which characterise the respective elasticity modulus. These values are assumed to be the momentary elasticity modulus E_0 when the description of the contact in next phase is realised. The parameters $\delta = 0.85$ and $t_0 = 1$ s are assumed. It is possible to observe the range and velocity of formation of RAC depends on time needed for contact formation until application of shear stress at friction. Of course the relationships between the quantities cannot be adequate to represent to reality, i.e., the characteristics of viscoelastic behaviour of the material at volumetric and shear deformations were selected accidentally. This is due to the fact that the time under shear at the transition from static contact to sliding is usually significantly shorter than the time under compression at the stationary contact. The result of visualisation of the process of the rheological increase of RAC as a function of time of contact before shear force and initiation of sliding is shown in Fig. 18.

5. Conclusions

It is clear that the assumption about the significant increase of intensity of RAC formation during acting of
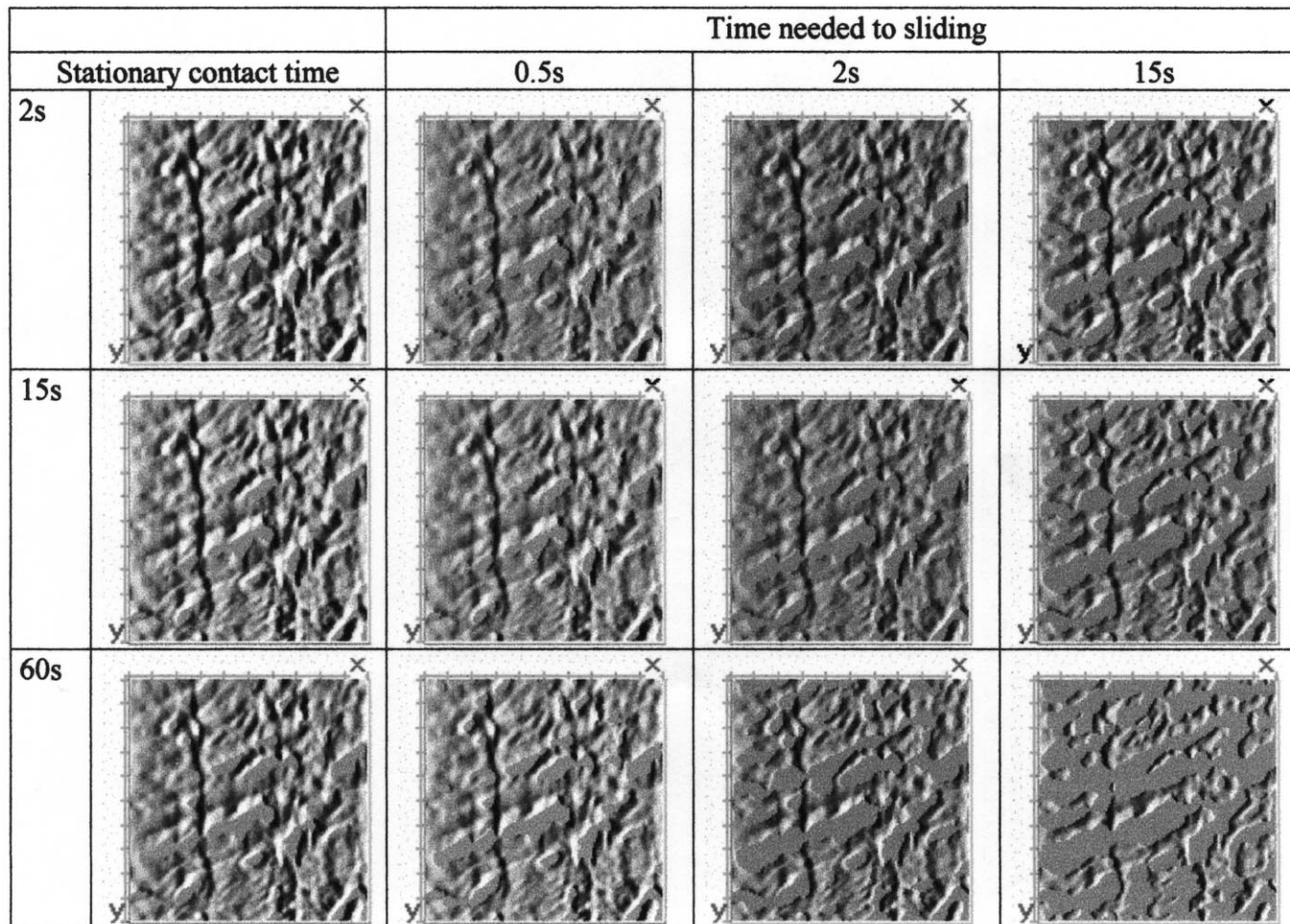
Fig. 18. Visualisation of contact area as a function of time of stationary contact before sliding and time needed for sliding; flat areas present the real area of contact.

shear force is not true. The experimental investigation has not shown a significant increase in $\Delta\mu$ when the time t_r needed to slide was increased. The preliminary displacement in the microbearing can increase when t_r is increased.

From the experimental results, the time needed for sliding t_r increases as time t_p of static contact before the initiation of shear stress is increased. The cause of such effect was not considered here. However, it is possible to assume that this effect is caused by the increase of the preliminary displacement, i.e., a characteristic length of elongation of the material aspirates until their damage, characterising the transition from static contact to sliding. The increase of the preliminary contact area is also caused by the change in the elasticity modulus because of the rheological deformation in contact.

The successful agreement between experimental and theoretical values in Figs. 15 and 16 was found. The trial to construct a model of the viscolastic microcontact with the application of the AFM images for the clarification of the time-dependent characteristics of polymer–polymer microbearings was effective in understanding the experimentally obtained results. The problem of further studies of rough surfaces viscoelastic contact which needs the estimation of the properties of the materials in very thin surface layers is open. For this purpose, it is necessary to find new and original test methods. One of possible solution of the problem is the application of AFM operating in dynamic contact mode.

References

[1] Z. Rymuza, Tribology of Miniature Systems, Elsevier, Amsterdam, 1989.

[2] Z. Rymuza, Tribology of Anti-Friction Polymers, WNT, Warszawa, 1986, in Polish.

[3] Z. Rymuza, Z. Kusznierewicz, G. Mañturzyk, Testing miniature, in particular polymer–polymer, journal bearings, Wear 174 (1994) 39–46.

[4] M. Mehregany, S.D. Senturia, J.H. Lang, P. Nagarkar, Micromotor fabrication, IEEE Trans. Electron Devices 39 (1992) 2060–2069.

[5] V.R. Dhuler, M. Mehregany, A.M. Phillips, A comparative study of bearing designs and operational environments for harmonic side-drive micromotors, IEEE Trans. Electron Devices 40 (1993) 1985–1989.

[6] U. Wallrabe, P. Bley, B. Krevet, W. Menz, J. Mohr, Design rules and test of electrostatic micromotors made by the LIGA process, J. Micromech. Microeng. 4 (1994) 40–45.

[7] P.J. Blau, Friction Science and Technology, Marcel Dekker, New York, 1996.

[8] S.A. Chizhik, V.V. Gorbunov, N.K. Myshkin, The analysis of molecular scale roughness effect on contact of solids based on computer modelling, Precis. Eng. 17 (1995) 186–191.

[9] Y. Yamaguchi, Tribology of Plastic Materials, Elsevier, Amsterdam, 1990.

[10] N.K. Myshkin, S.A. Chizhik, V.V. Gorbunov, Nanoscale topography and tribological problems, Tribol. Int. 28 (1995) 39–43.

[11] K.N.G. Fuller, D. Tabor, The effect of surface roughness on the adhesion of elastic solids, Proc. R. Soc. London A 345 (1975) 327–342.

[12] S.N. Magonov, Atomic Force Microscopy of polymers and related compounds, Vysokomolekularnye Soyedinenya Series B 38 (1996) 143–182, in Russian.